# Numerical Modelling of Reverse Flow Phenomena in a Channel with Obstruction Geometry at the Entry

**M.A. Kabir[1], M.M. K. Khan[2] AND M. G. Rasul[2]**
[1]Department of Mechanical Engineering, Carnegie Mellon University, Pittsburgh, PA 15213, USA
Email:kabira@andrew.cmu.edu
[2]College of Engineering and Built Environment, Faculty of Sciences, Engineering and Health, Central Queensland University, Rockhampton, QLD-4702, Australia

*Abstract:* - Numerical modelling and simulation of the reverse flow phenomenon in a channel with obstruction geometry at the entry were performed using CFD-ACE+ simulation solver. Obstruction geometries used for simulation were triangle, circle, semicircle and flat plate. Simulations were performed for different gap to width ratio, for different gap between the test channel and obstruction geometry, and for different Reynolds number. The simulated results are discussed and compared with flow visualization images. Simulations results predicted the occurrence of reverse flow and existence of other flow features such as vortex shedding at both ends. The numerically predicted results of the flow phenomena are generally in good agreement with the experimentally observed flow visualization images.

*Keywords:* - Reverse Flow, Test Channel, Obstruction, Flow Visualization and Simulation

## 1 Introduction

Reverse flow phenomenon has significant importance and can be employed in the control of energy and various flows in the process engineering applications [1]. There are several other applications where these reverse flow phenomenon can occur or can be employed such as: in flow control to achieve low velocities; shear layer interaction at varying distance apart; heat transfer applications to provide different types of flows locally; flow past obstruction and constrictions in arterial flows under certain physiological conditions [1, 2].

Reverse flow can occur in a channel when a obstruction geometry is placed at the entry of the channel. This flow phenomenon involves separation, reattachment and shear layer interaction. There are several parameters that affect the reverse flow phenomenon [3]. These are: shapes and size of obstruction geometries (circle, triangle, semicircle, etc), gap (g) between the obstruction and the test channel, length (L) of the test channel, Reynolds number (Re) and width (w) of the test channel. Gowda *et al.* [2] carried out extensive experimental investigation of the flow in a channel with various obstruction geometries (flat plate, circle, semicircle and triangle) at the entry. Experimental studies, however, are time consuming and expensive and may be even impossible in some geometries and applications. Computational fluid dynamics (CFD) provides cheaper alternative to experimental study. However, only a limited number of studies on numerical simulation have been found in the literature where Dijali *et al.* [4] predicted the turbulence flow around a bluff rectangular plate, Tafti [5] predicted flow field on a blunt plate and Ali *et al.* [6] predicted the three-dimensional flow field around circular cylinder. Tafti [5] showed a flow separation and reattachment on blunt plate.

The aim of the present study is to simulate the reverse flow phenomenon which involves flow separation and vortex pairing. The obstruction geometries used in this study were triangle, semicircle, rectangle (flat plate) and triangle. Among all the flow parameters, the shapes and sizes of obstruction geometries, the gap between the test channel and the obstruction geometry and the Reynolds number have shown a stronger influence on the flow field. Therefore, numerical simulations involving these three flow parameters are presented.

## 2 Governing Equations

The flow domain is shown in Figure 1. It is the same domain as considered for the flow visualization studies by Kabir *et al.* [3]. The flow through and around the test channel was computed by solving the unsteady Navier-Stokes equations for incompressible fluid in a two-dimensional geometry. The continuity and Navier-Stokes equations in general form for two dimensional flows are respectively given by,

$$\frac{\partial u}{\partial x}+\frac{\partial v}{\partial y}=0 \qquad (1)$$

$$\rho\left(\frac{\partial u}{\partial t}+u\frac{\partial u}{\partial x}+v\frac{\partial u}{\partial y}\right)=-\frac{\partial p}{\partial x}+\mu\left(\frac{\partial^2 u}{\partial x^2}+\frac{\partial^2 u}{\partial y^2}\right) \qquad (2)$$

$$\rho\left(\frac{\partial v}{\partial t}+u\frac{\partial v}{\partial x}+v\frac{\partial v}{\partial y}\right)=-\frac{\partial p}{\partial y}+\mu\left(\frac{\partial^2 v}{\partial x^2}+\frac{\partial^2 v}{\partial y^2}\right) \qquad (3)$$

The three unknowns in this model are *u*, *v* and, *p* and we have three equations to determine these unknowns. There are a total of six independent and dependent variables, and their nondimensional counter parts are obtained by dividing each quantity by its corresponding characteristics dimension. Using an asterisk to denote a nondimensional quantity, it can be written as:

$$x^*=\frac{x}{L},\quad y^*=\frac{y}{L},\quad t^*=\frac{t}{T},\quad u^*=\frac{u}{U},\quad v^*=\frac{v}{U},$$

$$p^*=\frac{p}{P}$$

To make these equations dimensionless, we must have to derive the nondimensional form of various time and space derivates. The time derivatives with respect to the dimensional variable can be written as:

$$\frac{\partial(\ )}{\partial t}=\frac{\partial(\ )}{\partial t^*}\frac{\partial t^*}{\partial t}=\frac{1}{T}\frac{\partial(\ )}{\partial t^*}$$

Similarly, the spatial derivates are given by

$$\frac{\partial(\ )}{\partial x}=\frac{\partial(\ )}{\partial x^*}\frac{\partial x^*}{\partial x}=\frac{1}{L}\frac{\partial(\ )}{\partial x^*},$$

$$\frac{\partial(\ )}{\partial y}=\frac{\partial(\ )}{\partial y^*}\frac{\partial y^*}{\partial y}=\frac{1}{L}\frac{\partial(\ )}{\partial y^*}$$

and, $\frac{\partial^2(\ )}{\partial x^2}=\frac{1}{L^2}\frac{\partial^2(\ )}{\partial x^{*2}}$,

$$\frac{\partial^2(\ )}{\partial y^2}=\frac{1}{L^2}\frac{\partial^2(\ )}{\partial y^{*2}}$$

Thus continuity equation becomes

$$\frac{\partial u}{\partial x}+\frac{\partial v}{\partial y}=\frac{1}{L}\frac{\partial(u^*U)}{\partial x^*}+\frac{1}{L}\frac{\partial(v^*U)}{\partial y^*}=0$$

$$\frac{U}{L}\left(\frac{\partial u^*}{\partial x^*}+\frac{\partial v^*}{\partial y^*}\right)=0 \qquad (4)$$

The nondimensional form of continuity equation is given by,

$$\frac{\partial u^*}{\partial x^*}+\frac{\partial v^*}{\partial y^*}=0 \qquad (5)$$

Using similar process, nondimensional Navier-Stokes equations can be given by,

$$\left(\frac{L}{UT}\right)\frac{\partial u^*}{\partial t^*}+u^*\frac{\partial u^*}{\partial x^*}+v^*\frac{\partial u^*}{\partial y^*}=-\left(\frac{P}{\rho U^2}\right)\frac{\partial p^*}{\partial x^*}+\left(\frac{\mu}{\rho UL}\right)\left(\frac{\partial^2 u^*}{\partial x^{*2}}+\frac{\partial^2 u^*}{\partial y^{*2}}\right)$$

$$\left(\frac{L}{UT}\right)\frac{\partial v^*}{\partial t^*}+u^*\frac{\partial v^*}{\partial x^*}+v^*\frac{\partial v^*}{\partial y^*}=-\left(\frac{P}{\rho U^2}\right)\frac{\partial p^*}{\partial y^*}+\left(\frac{\mu}{\rho UL}\right)\left(\frac{\partial^2 v^*}{\partial x^{*2}}+\frac{\partial^2 v^*}{\partial y^{*2}}\right)$$

There are three dimensionless groups in the non-dimensional Navier-Stokes equations, these are:

$$\frac{L}{UT},\ \frac{P}{\rho U^2}\ \text{and}\ \frac{\mu}{\rho UL}$$

Therefore the continuity and Navier-Stokes equations in dimensionless form for two dimensional channel flow where width (w) of channel is the characteristics length (*L*) and U is the free stream uniform velocity at the entry of the test channel. Here μ is the dynamic viscosity; ρ is the density of the fluid, and Re is the Reynolds number. The continuity and momentum equations in dimensionless form can be written as,

$$\frac{\partial u}{\partial x}+\frac{\partial v}{\partial y}=0 \qquad (6)$$

$$\frac{\partial u}{\partial t}+u\frac{\partial u}{\partial x}+v\frac{\partial u}{\partial y}=-\frac{\partial p}{\partial x}+\frac{1}{\mathrm{Re}}\left(\frac{\partial^2 u}{\partial x^2}+\frac{\partial^2 u}{\partial y^2}\right) \qquad (7)$$

$$\frac{\partial v}{\partial t}+u\frac{\partial v}{\partial x}+v\frac{\partial v}{\partial y}=-\frac{\partial p}{\partial x}+\frac{1}{\mathrm{Re}}\left(\frac{\partial^2 v}{\partial x^2}+\frac{\partial^2 v}{\partial y^2}\right) \qquad (8)$$

The variables were made dimensionless as defined below by using U and w, followed by dropping the asterisks:

$$x^* = \frac{x}{w}, y^* = \frac{y}{w}, t^* = \frac{TU}{w}, p^* = \frac{P}{\rho U^2}, u^* = \frac{u}{U},$$

$$v^* = \frac{v}{U} \text{ and } Re = \frac{Uw\rho}{\mu}$$

## 3 Computational Model and Boundary Conditions

The two dimensional computational fluid dynamics (CFD) model of the test channel with different obstruction geometries at the entry placed in another wider parallel walled channel was developed using commercially available software, CFD-ACE (CFD Research Corp., Huntsville, AL). The CFD-ACE+ code used were based on a finite volume method. The flow domain was discretized using unstructured grid. Computational flow simulations of this type are based on the division of the flow domain into small (finite) volumes. The symmetry assumption was used for solution in the test channel section of the flow field. Several trails were made to eliminate the dependence of grid on the numerical simulation. The mesh consists of 3186 cells in the half domain with an increased density of cells at the test channel sections.

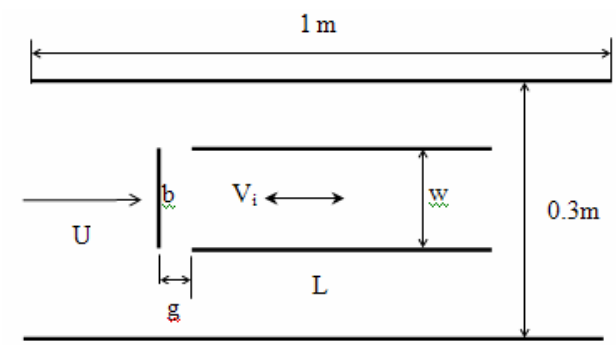


Fig. 1 Computational flow domain

The length and width of the wider channel of the test section were 1 m x 0.3 m as shown in Fig. 1 and used for flow simulations in this study. The widths of the test channel (w) and the obstruction geometry (b) were constant and equal to 25 mm same as that of experimental set up. The obstruction geometries were located at the entry of the test channel at varying gap (g) to width (w) ratios from 0.5 to 8.0. The free stream velocity (U) in the wider channel were fixed from 0.04 m/s, 0.12 m/s, 0.24 m/s and 0.36 m/s and the corresponding Reynolds number of these velocities were 1000, 3000, 6000 and 9000. The simulations to study the influence of the shapes of the obstruction geometries were carried out at a fixed Reynolds number of 6000, whereas the simulations for the influence of the gap between the obstruction and the test channel were performed for Re of 1000 to 9000.

The domain used in this numerical prediction of flow behavior inside and around the test channel is shown in Fig. 2. This is the same domain, used for experimental investigations of the flow phenomena of water. The flow inside and around the test channel was computed for water (incompressible fluid) in a two-dimensional geometry. Volume, boundary and initial conditions were given in CFD-ACE solver for the simulation of the flow phenomena. The volume conditions were 1) incompressible fluid (water) for all domains except obstruction and test channel domain; 2) obstruction and test channel domain are blockage.

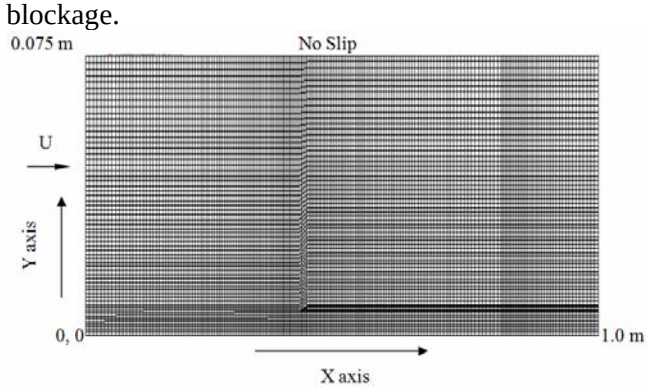


Fig. 2 Computational domains for the numerical prediction of flow

The boundary conditions were: no slip condition on; (1) the walls of the wider channel, (2) the walls of the test channel, (3) the walls of the obstruction geometry and (4) the uniform velocity at the entrance of the domain. The velocities *u* and *v* (in x and y directions) were small typically $10^{-6}$ m/s as initial conditions for all domains. The temperature for simulations was kept at 25°C same as used for the experimental investigation of the flow phenomena. The Reynolds number Re was based on the free stream velocity (U), water density (ρ), and viscosity (μ) on the width (w) of the test channel. Post processing of the results includes calculation of the velocity ratio inside and free stream ($V_i$/U: inside

velocity/free stream velocity) velocities in the test channel for different obstruction geometries.

# 4 Results and Discussion

## 4.1 Simulations of Shapes of Obstruction Geometry

Numerical predictions of the flow phenomena of water were performed for g/w ratios of 0.5, 1.0, 1.4, 2.0, 4.0 and 6.0. It was observed from the experimental investigation that various obstruction geometries (except flat plate) produced the maximum reverse flow at g/w ratio of 0.5 [1]. Therefore, the numerical simulations for the g/w ratio of 0.5 are presented in Figures 3a-d for discussion and comparison. In the experimental investigation, the flow was observed unsteady at both entry and exit ends of the test channel. However, the flow was steady in the central portion of the test channel. The predicted velocity vectors and streamlines of the entry and exit end of the test channel are presented in Figures 3a-d. For a better comparison, the experimental flow visualization photographs of various obstruction geometries are also shown at the top half of those figures.

It can be seen from the numerically predicted velocity vectors and stream lines of various shaped geometries (Figures 3a-d) that the shear layers separating from the edges of the geometry reattached on the sidewalls of the test channel at low g/w ratios. It can also be seen (Figures 3a-d) that a low pressure zone is created at the gap between the test channel and the obstruction geometry which triggers the flow in the reverse direction. The details experimental study of the flow phenomena in a channel with obstructions with various geometries was published elsewhere [3]. It was seen that a flow separation took place at the entrance of the channel and the vortex shedding occurs at channel ends. The shear layers at the front and rear ends on both sides of the channel become unstable and roll up giving rise to complex vortex shedding. The vortex shedding near the entrance and exit causes the flow to enter and leave the test channel as can be seen in Figures 3a-d. The same vortices at the channel ends were observed for the experimental investigations [3]. This vortex regulates the flow of the water through the test channel. The magnitude of the reverse flow is determined by the combination of the low pressure behind the obstruction and the vortex shedding [2].

The predicted velocity vectors and stream lines of the reverse flow inside the test channel match well with the streak lines of the flow visualization photographs. The predicted vortices observed at both ends for triangle and flat plate obstruction geometry are in good agreement with that of flow visualization pictures (Figures 3a and 3d). For circle, the simulated velocity vectors and streamlines are in moderate agreement with the streak lines of flow visualization images (Figure 3b).

The flat plate obstruction due to its shape acts as shield and protects the adjacent negative pressure zone from the surrounding forward flow environment whereas, the obstruction geometries namely circle, semicircle and triangle due to their shapes were unable to protect the negative pressure zone as effectively as flat plate in particular when the g/w ratio increased; therefore, the negative pressure zone was dominant for flat plate. The higher the negative pressure, the stronger the reverse flow was inside the test channel. The magnitudes of the reverse flow obtained from numerical simulations, where simulated velocity vectors and stream lines are in good agreement with the flow visualization images, were seen to vary within 10% to 12% from the experimental value. The general agreement in the quantitative and qualitative simulation results was observed for triangle, circle, semicircle and flat plate with that of the experimental results published elsewhere [3].

## 4.2 Simulation of Gap

Numerical predictions for g/w ratios of 0.5, 1.0 and 1.5 are presented and discussed here. These g/w ratios were selected because it was observed from the experimental investigation that (a) an appreciable reverse flow was produced at g/w ratio of 0.5 (b) a moderately high reverse flow was produced at g/w ratio of 1.0 (c) a maximum reverse flow was produced at g/w ratio of 1.5. The simulated velocity vectors and streamlines of the g/w ratios are shown in Figures 4a-c. The numerically predicted velocity vectors and streamlines are generally in agreement with the streak lines of the flow visualization pictures. The predicted magnitudes of the reverse flow were found to vary within 10% to 12% from the experimental value. Appreciable magnitude of the predicted reverse flow was seen at low g/w ratio of 0.5.

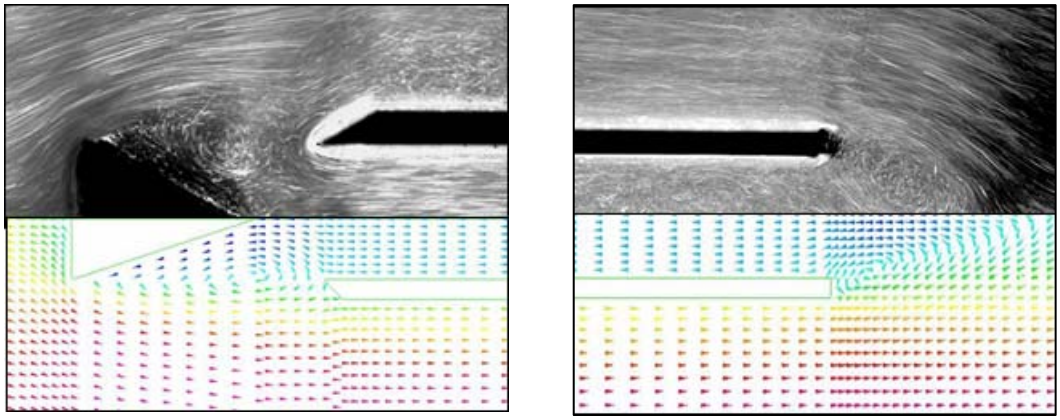

Figure 3a: Flow with triangle at g/w =0.5, time step = 36, Re = 6000 and L/w = 8.0

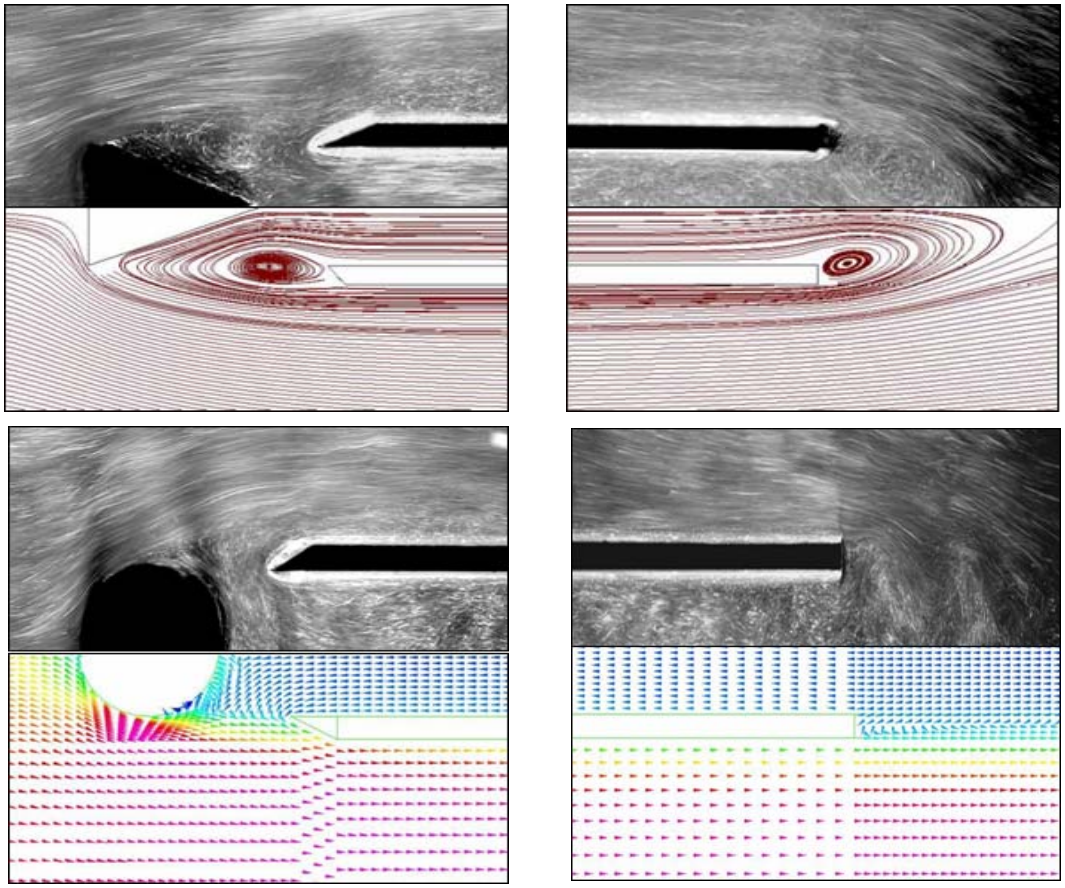

Figure 3b: Flow with circle at g/w =0.5, time step = 33, Re = 6000 and L/w = 8.0

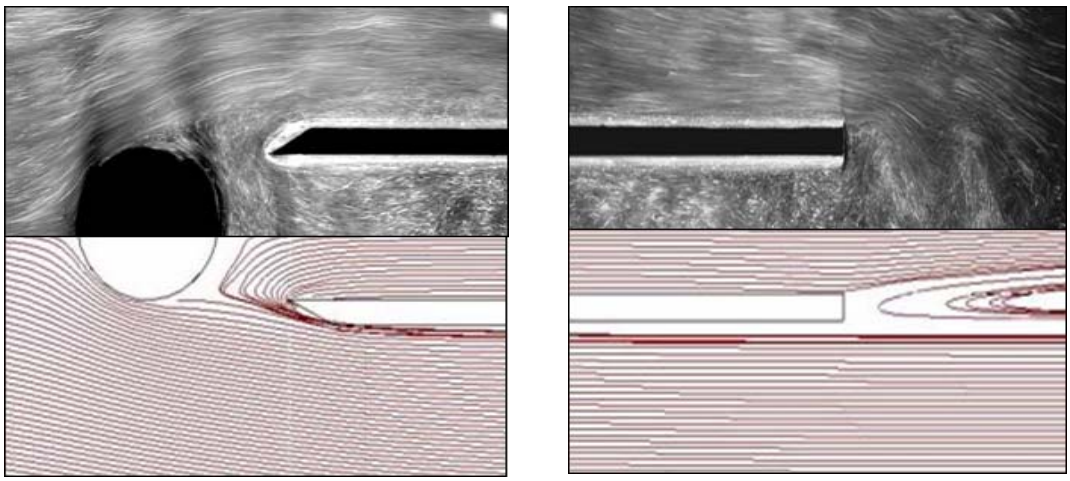

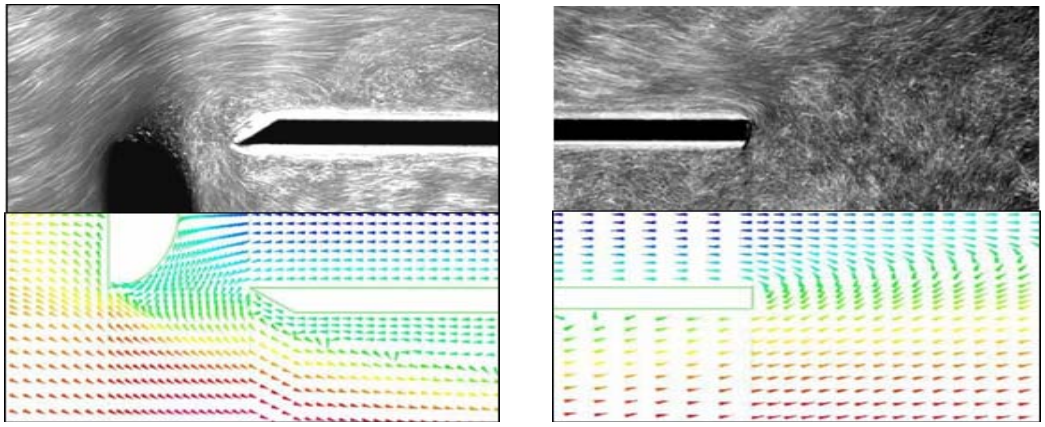

Figure 3c: Flow with semicircle at g/w =0.5, time step=36, Re = 6000 and L/w = 8.0

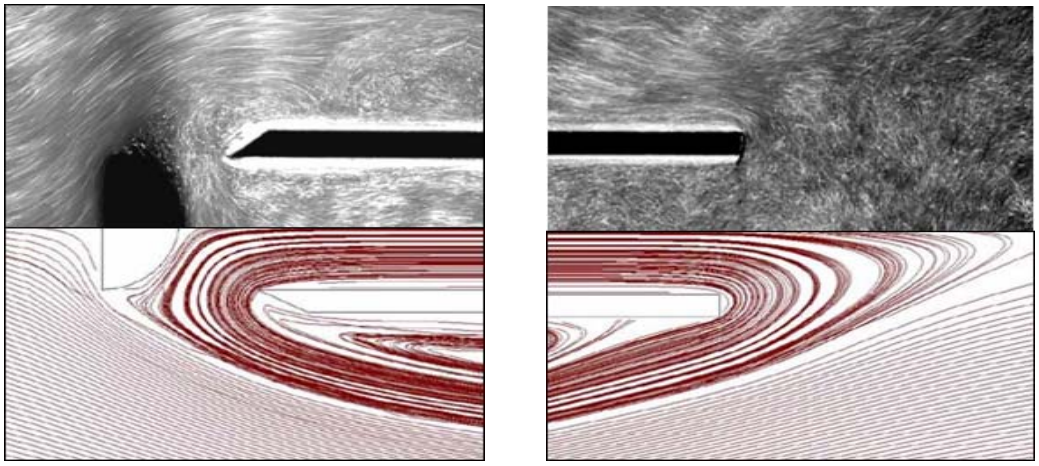

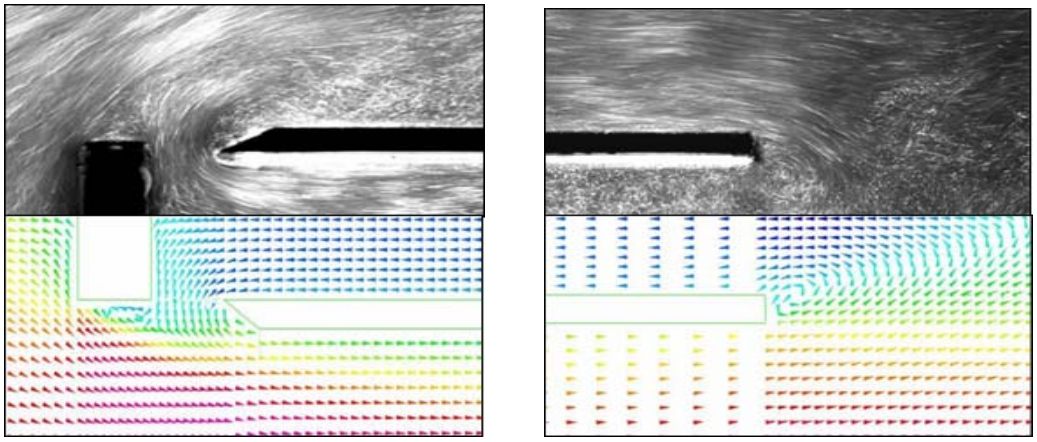

Figure 3d: Flow with circle at g/w =0.5, time step = 33, Re = 6000 and L/w = 8.0

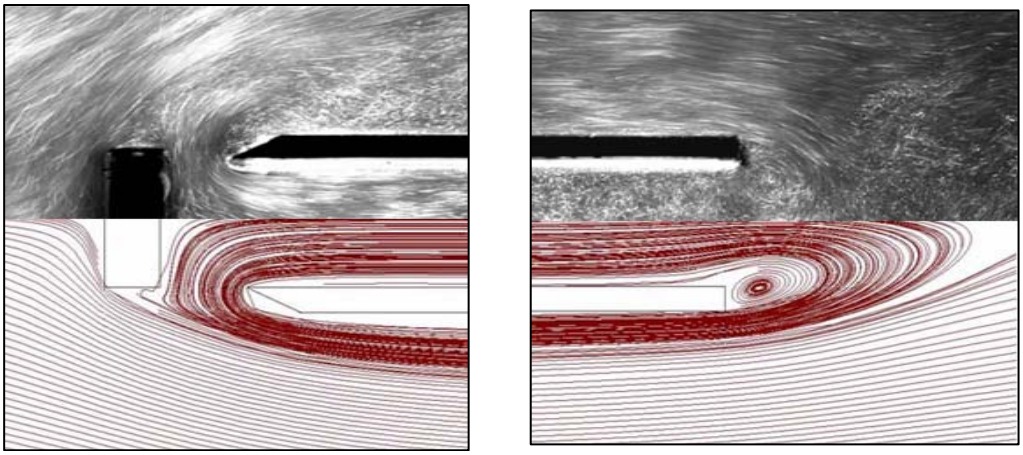

Figure 3a-d: Flow visualization pictures showing steak lines at the top and predicted velocity vectors and streamlines at the bottom for water.

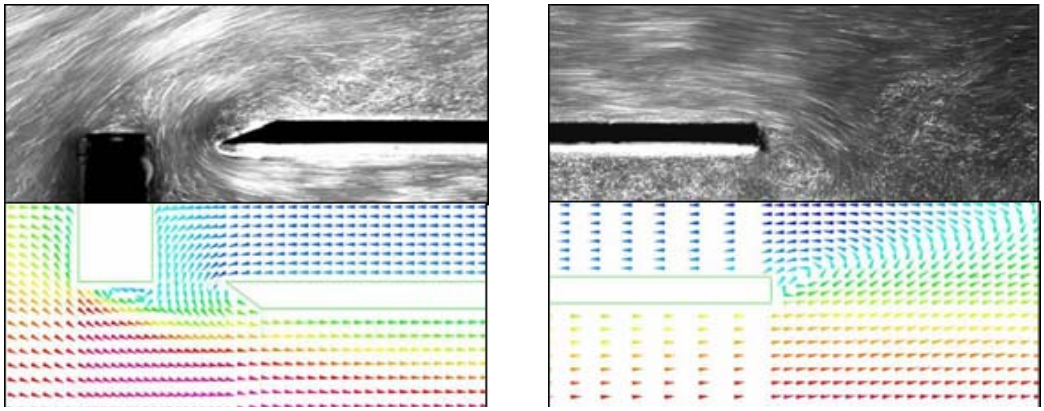

4a. g/w = 0.5, time step = 35, Re = 6000 and L/w = 8.0

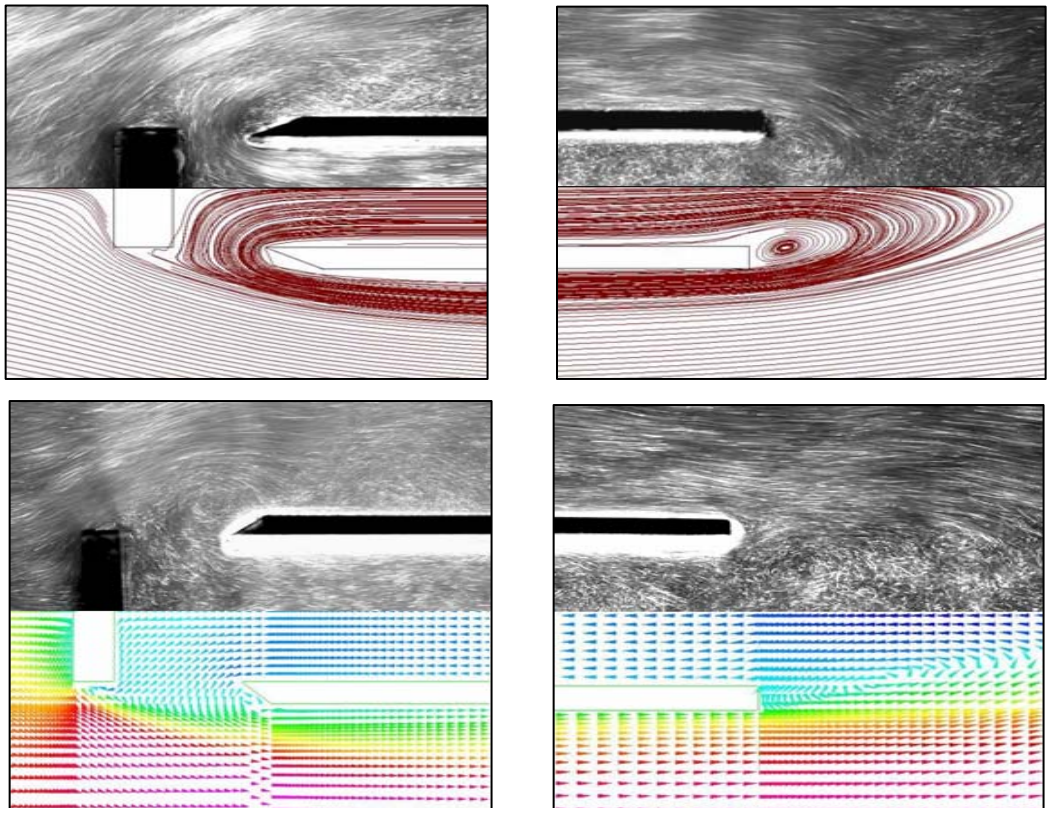

4b. g/w = 1.0, time step = 33, Re = 6000 and L/w = 8.0

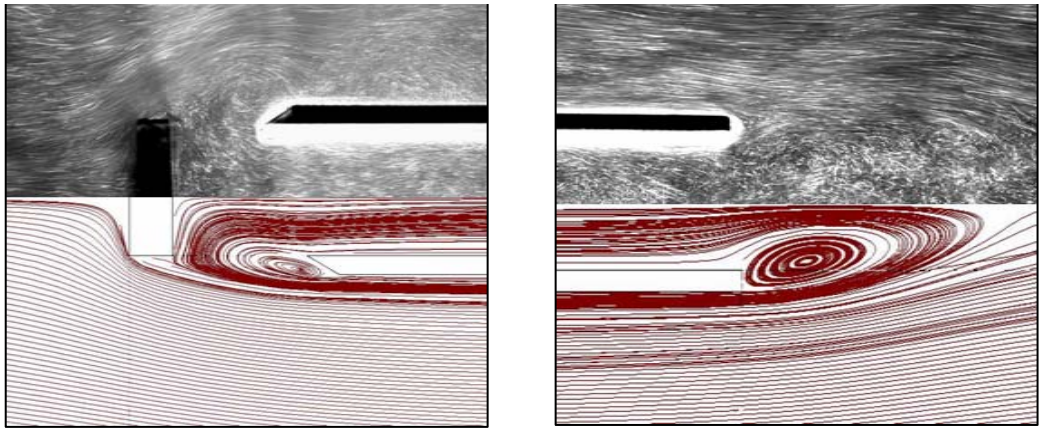

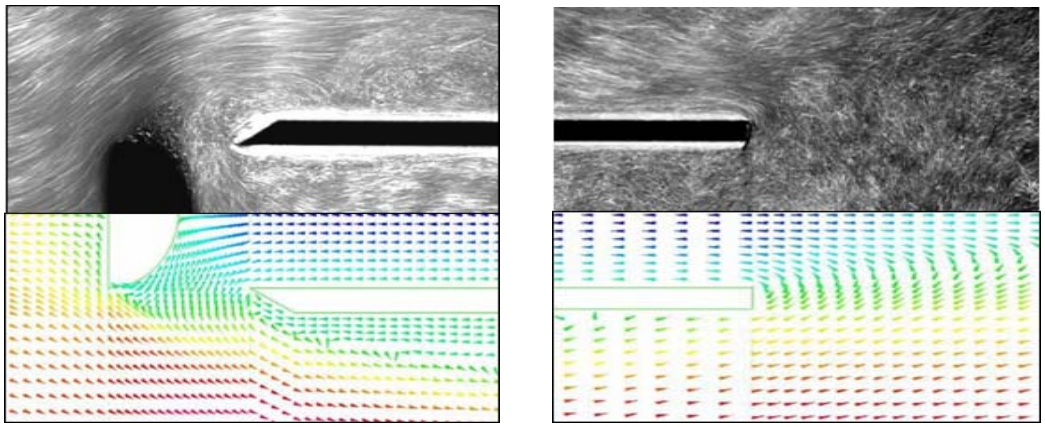

Figure 3c: Flow with semicircle at g/w =0.5, time step=36, Re = 6000 and L/w = 8.0

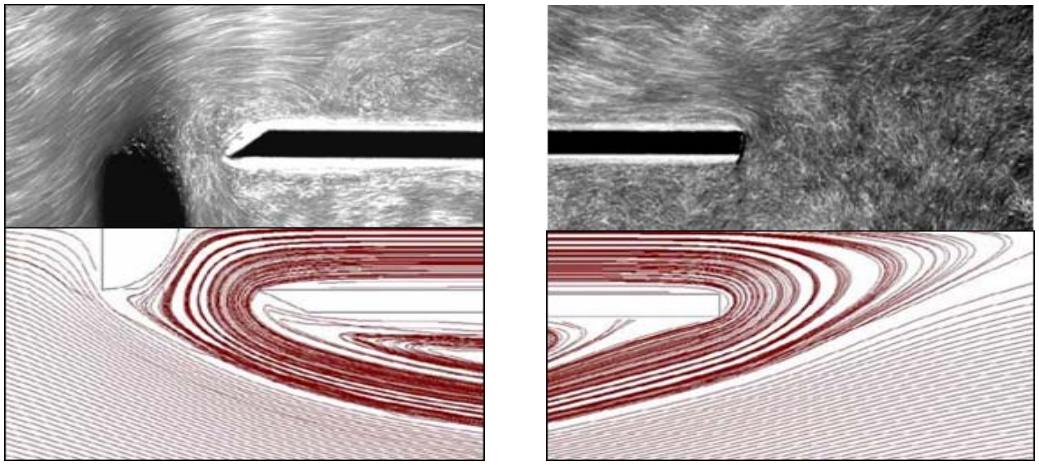

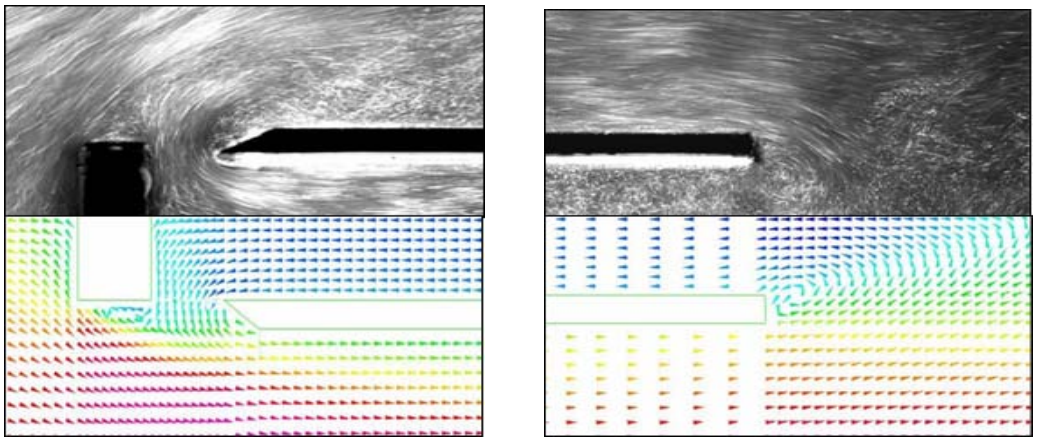

Figure 3d: Flow with circle at g/w =0.5, time step = 33, Re = 6000 and L/w = 8.0

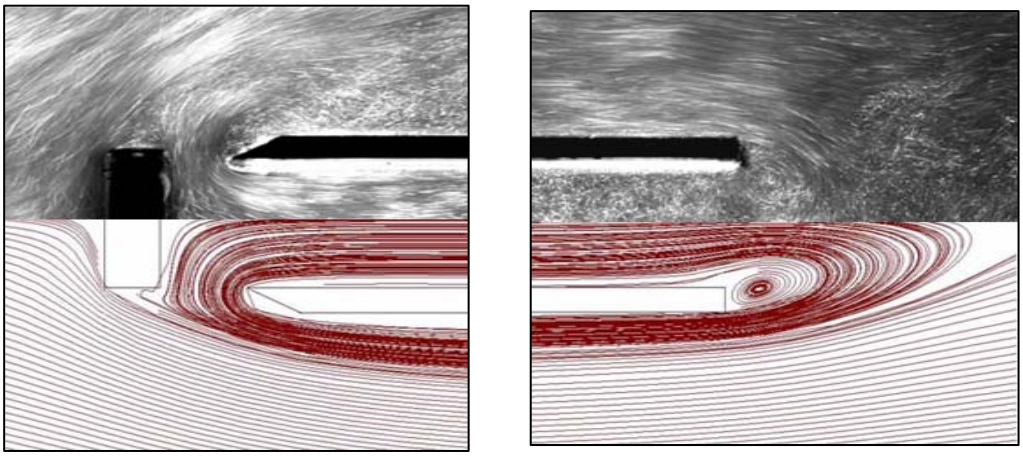

Figure 3a-d: Flow visualization pictures showing steak lines at the top and predicted velocity vectors and streamlines at the bottom for water.

g/w ratio of 1.0 and L/w ratio of 8.0. It can be seen from Figures 5a-b that as Reynolds number increases; vortices disappear (vortex breakdown takes place). The similar flow phenomena were observed in flow visualization pictures for water. It was found that the predicted magnitude of the reverse flow is within 10%-12% variation with the experimental velocity magnitude. The overall predicted velocity vectors and streamlines of reverse flow inside the test channel at Reynolds numbers of 1000 and 3000 show a good match with the flow pattern. The vortex appearing at the exit end is smaller in size and it has some agreements with that of simulated velocity vectors and stream lines. It can also be observed that for the Reynolds number of 9000, the predicted velocity vectors and streamlines are in good agreement with that of the experimental flow visualization image (Figure 5c). The predicted velocity vectors and streamlines in Figures 5a-b also show vortices which are in agreement with the flow visualization pictures showing streak lines vortices.

## 5 Conclusions

The numerical simulation of the reverse flow phenomena in a channel with obstruction geometry is performed by solving the Navier-stokes equations for water. The influence of the flow parameters namely, the shapes of the obstruction geometry, the gap between the test channel and the obstruction geometry, and the Reynolds number are studied. It was found that for various shapes and sizes, simulated velocity vectors and streamlines are in good agreement with the streak lines of the flow visualization photographs. Numerical simulations were carried out at g/w ratios of 0.5, 1.0 and 1.5 for Reynolds number of 6000. It was found that the simulated velocity vectors and streamlines show a good agreement with that of streak lines of the flow visualization pictures. For g/w ratio of 1.0, numerical simulations were carried out for Reynolds numbers of 1000, 3000 and 9000. The simulated vortices of the flow pattern for all the cases show a fair to good agreement with that of the flow visualization vortices. It was seen that the predicted vortices of both ends of the channel are in good agreement with that of the visualization image vortices. The numerically predicted magnitude of the velocity inside and around the test channel was found to vary within 10% to 12% of the experimental value. The numerical simulations performed for shapes, Reynolds numbers and the gap indicates that the developed model should be capable of predicting the flow behavior of any other shapes of obstruction geometry.

***References***

[1] Kabir, M.A., Flow characteristics of Newtonian and non-Newtonian fluids in a channel with obstruction at the entry, PhD Thesis, Faculty of Sciences, Engineering and Health, 2004, Central Queensland University.

[2] Gowda, B. H. L., Tulapurkara, E. G. and Swain, S.K, Reverse flow in a channel influence of obstruction geometry, Experiments in Fluids, 16, 1993, p137-145.

[3] Kabir, M. A, Khan, M. M. K. and Bhuiyan, M.A, Flow phenomena in a channel with different shaped obstructions at the entrance, Fluid Dynamics Research, 35, 2004, p391-408.

[4] Dijali, N., Gartshore, I.S. and et al., Turbulence flow around a bluff rectangular plate. Part II: Numerical predictions, Journal of Fluids Engineering, 113, 1991, P60-67.

[5] Tafti, D. K. and Vanka S. P, A numerical study of flow separation and reattachment on a blunt plate, Physics of Fluids, 3, 1991, p1749-1759.

[6] Ali, K. H. M. and Karim, O, Simulation of flow around piers, Journal of Hydraulic Research, 40, 2002, P161-174.

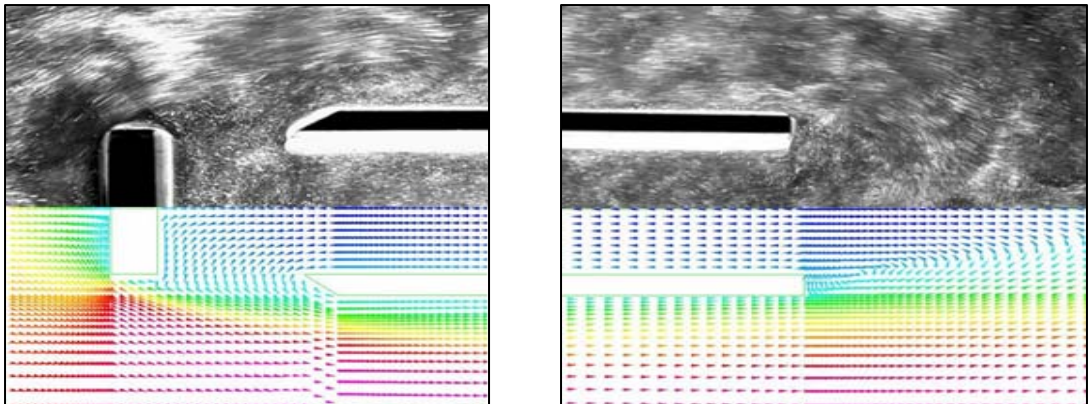

5a. Re = 1000, L/w = 8.0, time step = 24, g/w = 1

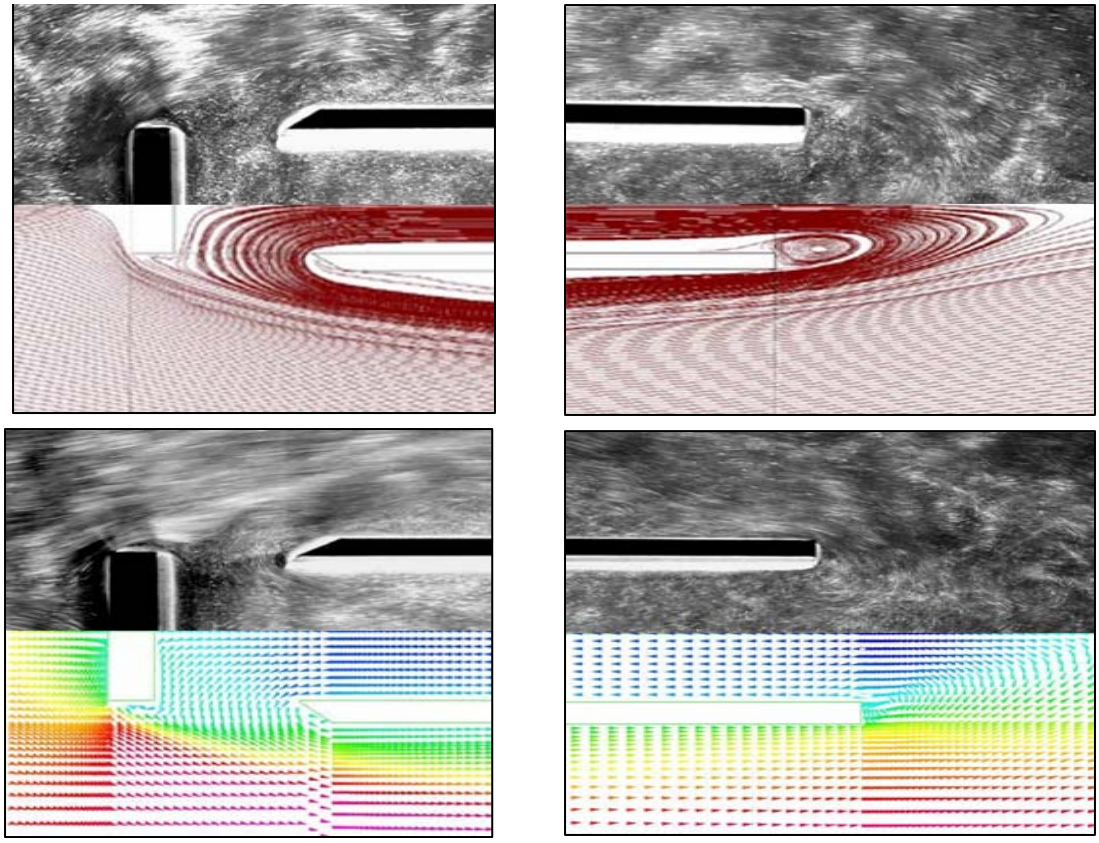

5b. Re = 3000, L/w = 8.0, time step = 35, g/w = 1

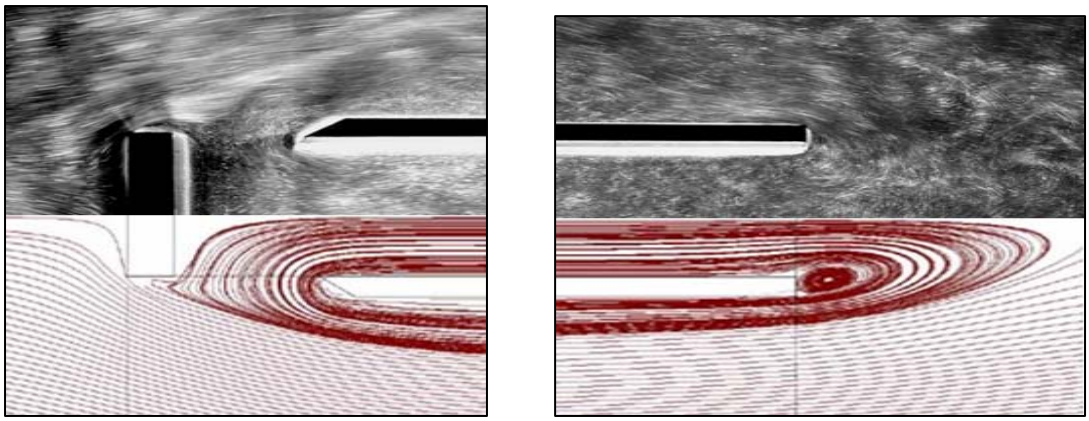

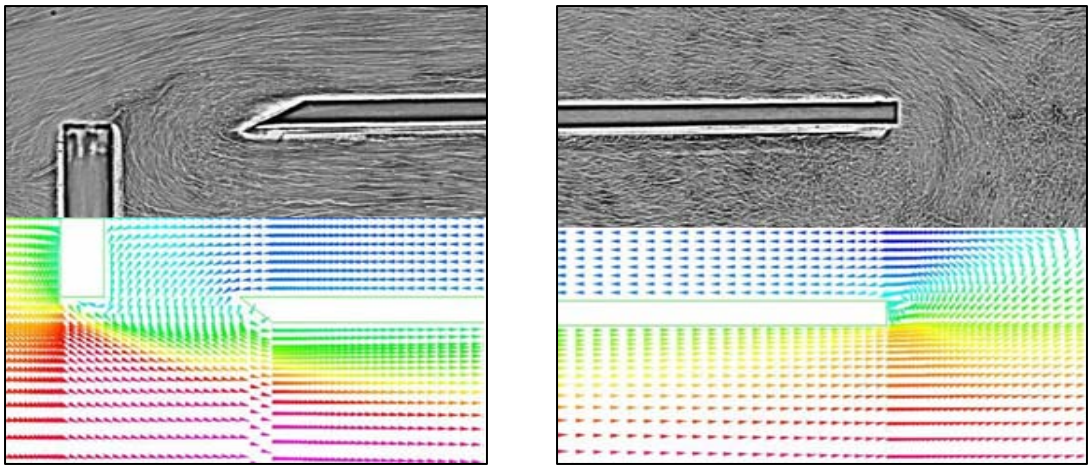

5c. Re = 9000, L/w = 8, time step = 27, g/w = 1

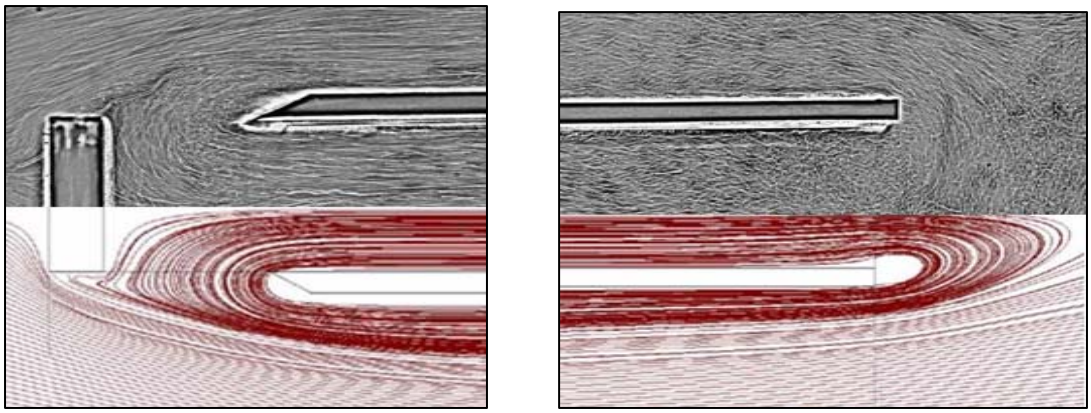

Figure 5a-c: Flow visualization pictures showing steak lines at the top and predicted velocity vectors and streamlines at the bottom for water.